Please cite this article in press as: Cheng et al., Perivascular Mast Cells Dynamically Probe Cutaneous Blood Vessels to Capture Immunoglobulin E, Immunity (2013), http://dx.doi.org/10.1016/j.immuni.2012.09.022

Immunity
Article

Perivascular Mast Cells Dynamically Probe Cutaneous Blood Vessels to Capture Immunoglobulin E

Laurence E. Cheng,[1] Karin Hartmann,[4] Axel Roers,[5] Matthew F. Krummel,[2] and Richard M. Locksley[3,*]
[1]Department of Pediatrics
[2]Department of Pathology
[3]Department of Medicine, Department of Microbiology and Immunology, and the Howard Hughes Medical Institute
University of California, San Francisco, San Francisco, CA 94143, USA
[4]Department of Dermatology, University of Cologne, 50937 Cologne, Germany
[5]Institute for Immunology, University of Technology Dresden, Medical Faculty Carl-Gustav Carus, 01307 Dresden, Germany
*Correspondence: locksley@medicine.ucsf.edu
http://dx.doi.org/10.1016/j.immuni.2012.09.022

SUMMARY

Mast cells are tissue-resident immune cells that play a central role in allergic disease. These contributions are largely dependent on the acquisition of antigen-specific immunoglobulin E (IgE). Despite this requirement, studies of mast cell and IgE interactions have overlooked the mechanism by which mast cells acquire IgE from the blood. To address this gap, we developed reporter IgE molecules and employed imaging techniques to study mast cell function in situ. Our data demonstrate that skin mast cells exhibit selective uptake of IgE based on perivascular positioning. Furthermore, perivascular mast cells acquire IgE by extending cell processes across the vessel wall to capture luminal IgE. These data demonstrate how tissue mast cells acquire IgE and reveal a strategy by which extravascular cells monitor blood contents to capture molecules central to cellular function.

INTRODUCTION

Mast cells are hematopoietic, tissue-resident cells that have been considered to play diverse roles in host defense and immune regulation as well as a central role in allergic disease (Galli and Tsai, 2010; Gould and Sutton, 2008; Locksley, 2010). Despite these many potential roles, recent studies, by using mouse strains with targeted mast cell deletion, have primarily served to underscore the mast cell contribution to the clinical manifestations of allergic disease (Dudeck et al., 2011; Feyerabend et al., 2011).

The mast cell contribution to allergy is largely dependent on the acquisition of monomeric immunoglobulin E (IgE) on the surface of mast cells through expression of the high affinity IgE receptor (FcεRI) (Kraft and Kinet, 2007). Though FcεRI can be detected on the surface of mast cell precursors (Hallgren and Gurish, 2007), expression of FcεRI on tissue-resident mast cells increases proportionally with serum IgE titers, suggesting the tissue as a primary site of IgE acquisition (Kraft and Kinet, 2007; Yamaguchi et al., 1997). Once mast cells are loaded with IgE, subsequent antigen binding leads to crosslinking of FcεRI molecules and the immediate release of preformed mediators, such as histamine, as well as synthesis of lipid and protein mediators (Galli and Tsai, 2010).

Studies of the mast cell-IgE axis have focused on the regulation of IgE production as well as the clinical manifestations of hypersensitivity responses following antigen exposure. Few studies have examined how mast cells acquire unbound IgE. Defining the mechanism by which mast cells capture IgE will fill a gap in our understanding of the mast cell-IgE axis and may provide new therapeutic approaches to severe allergic disorders.

Although cell-bound IgE is found primarily in tissues, IgE production by plasma cells occurs mostly in the bone marrow, spleen, and lymph nodes (Luger et al., 2009; McMenamin et al., 1992; Talay et al., 2012; Yang et al., 2012). Thus, the localization of IgE production is anatomically distinct from sites of IgE acquisition and effector function. As the amount of surface-bound IgE by tissue mast cells directly reflects the size of the serum IgE pool (Kraft and Kinet, 2007), the vasculature acts as a conduit by which unbound IgE is distributed to tissue mast cells. The vasculature also acts as a potential barrier to IgE uptake and could thereby regulate IgE delivery to tissue sites.

Mast cells show a preference toward perivascular localization within tissue, wherein a majority of mast cells lie in close proximity to the basal side of the vessel wall (Galli and Tsai, 2010). We hypothesized that this preferential localization might position mast cells to acquire IgE by a mechanism that requires cells to surmount the endothelial barrier. By using reporter IgE molecules, in vivo imaging techniques, and mast cell reporter mice, we demonstrate that perivascular mast cells dynamically extend processes into the vascular compartment to selectively acquire IgE from the blood.

RESULTS

Heterogeneous IgE Uptake by Skin Mast Cells

Passive diffusion of blood-borne IgE across the vasculature has been considered to be the primary means by which tissue mast cells acquire IgE. However, we hypothesized a more active mechanism of IgE acquisition by mast cells, which would lead to selective uptake of IgE by a subset of mast cells. Supporting

Please cite this article in press as: Cheng et al., Perivascular Mast Cells Dynamically Probe Cutaneous Blood Vessels to Capture Immunoglobulin E, Immunity (2013), http://dx.doi.org/10.1016/j.immuni.2012.09.022

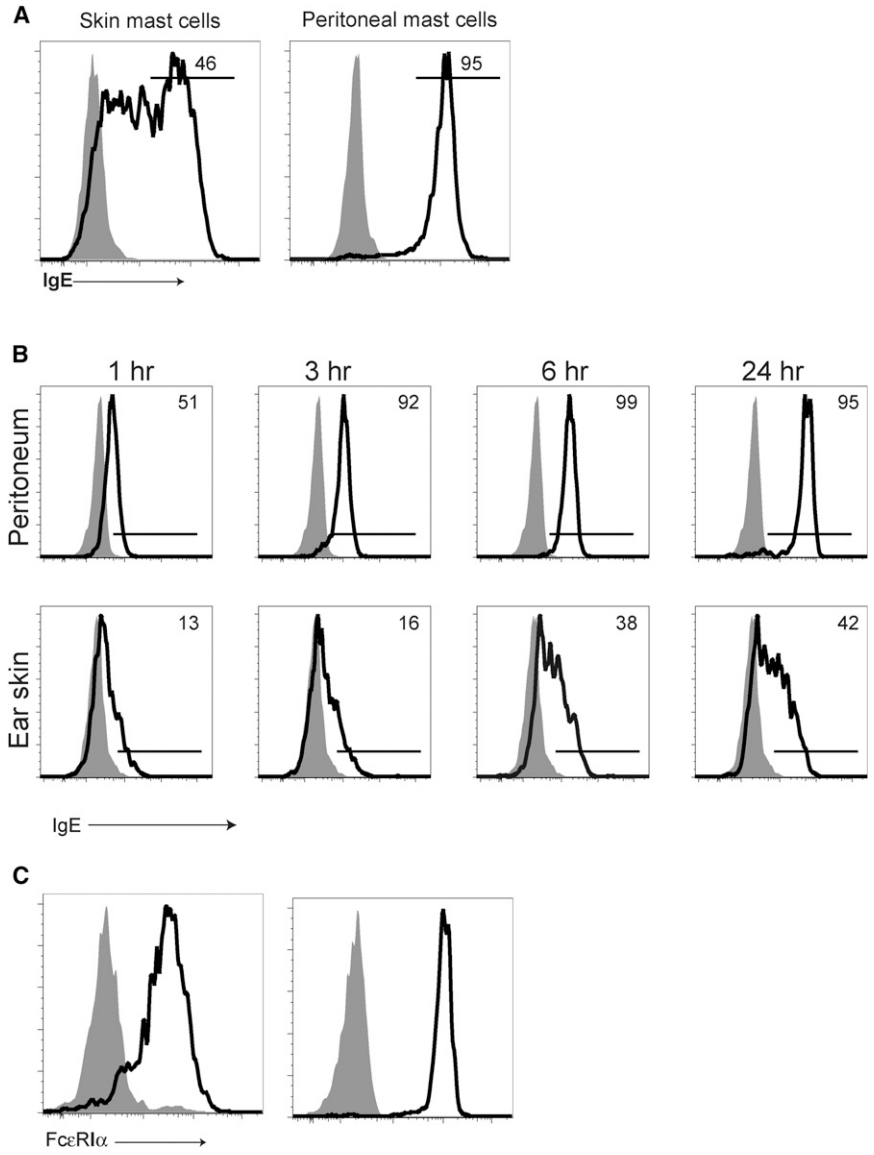

Figure 1. Heterogeneous Uptake of IgE from Blood by Skin Mast Cells

(A) Skin (left panel) and peritoneal (right panel) mast cells from 4get BALB/c mice were stained for IgE. Gray histograms represent IgE staining on mast cells from IgE-deficient 4getx*Rag2*$^{-/-}$ controls. Lines within histograms represent the percent of cells within the indicated gate.

(B) Peritoneal (top row) and ear skin mast cells (bottom row) from 4getx*Rag2*$^{-/-}$ mice were examined at the indicated times following a 10 μg i.v. infusion of monoclonal IgE. Histograms depict mast cell surface IgE. Shaded histograms represent control mice. The percent of IgE^{+} cells in the gated area of the histogram is also depicted. These data are representative of three independent experiments with two to three mice at each time point.

(C) Ear skin (left) and peritoneal (right) mast cells from 4getx*Rag2*$^{-/-}$ were stained with anti-FcεRI antibody. Gray histograms represent the isotype control. Results are representative of three mice for each plot.

See also Figure S1.

this idea, ear skin mast cells from 6-week old 4get BALB/c mice, in which mast cells constitutively express enhanced green fluorescent protein (eGFP) (see Figure S1A available online; Gessner et al., 2005), showed heterogeneous surface IgE with approximately 50% of the mast cells having high cell surface-bound IgE (Figure 1A). In contrast, peritoneal mast cells exhibited uniform cell-surface IgE. These differences were not a result of the protease-dependent skin mast cell isolation protocol as protease-treated peritoneal mast cells showed no loss of surface IgE (Figure S1B).

Mast cell-bound IgE has a half-life of up to 2 weeks and can modulate mast cell expression of FcεRI (Gould and Sutton, 2008; Yamaguchi et al., 1997). Therefore, we examined IgE uptake in IgE-deficient 4getx*Rag2*$^{-/-}$ mice following intravenous (i.v.) infusion of 10 μg of IgE. Despite peak IgE titers more than 50-fold greater than physiologic levels in IgE-replete animals (data not shown), only a select population of ear skin mast cells demonstrated IgE uptake at 1 hr and continued to accumulate IgE throughout the time course (Figure 1B). In contrast, peritoneal mast cells showed uniform uptake of IgE at 1 hr and further accumulation of IgE throughout the time course, similar to profiles seen at steady state in wild-type (WT) animals. The ear skin mast cells also did not demonstrate surface IgE staining commensurate with peritoneal mast cells. Although slightly lower than on peritoneal mast cells, FcεRI expression on skin mast cells could not account for this discrepancy (Figure 1C). Similar results were obtained with a smaller 1 μg infusion but with markedly lower IgE uptake in the ear (Figure S1C). Together, these data suggested that skin blood vessels regulate IgE trafficking into the tissue and that select mast cell populations had greater access to vascular contents. The data predicted that IgE uptake would similarly localize to perivascular mast cells.

Characterization of Reporter IgE Molecules and Localization of IgE Uptake

To visualize IgE uptake in tissues, we constructed a reporter IgE molecule consisting of a tandem red fluorescent protein (tdRFP) fused N-terminal to the Cε2–Cε4 domains of the IgE heavy chain (Cheng et al., 2010). The resulting homodimeric surrogate IgE molecule has a similar molecular weight as native IgE (188 kDa versus ~200 kDa for native IgE). After an i.v. infusion, RFP-Fcε was found on the cell surface of FcεRI^{+} cells, including splenic basophils and peritoneal mast cells (Figure 2A). Additionally, gating of peritoneal exudate cells and total splenocytes on RFP^{+} cells revealed that essentially all of these cells were mast cells or basophils, respectively (Figure 2B). Similar to data with native IgE, only a subset of skin mast cells captured RFP-Fcε

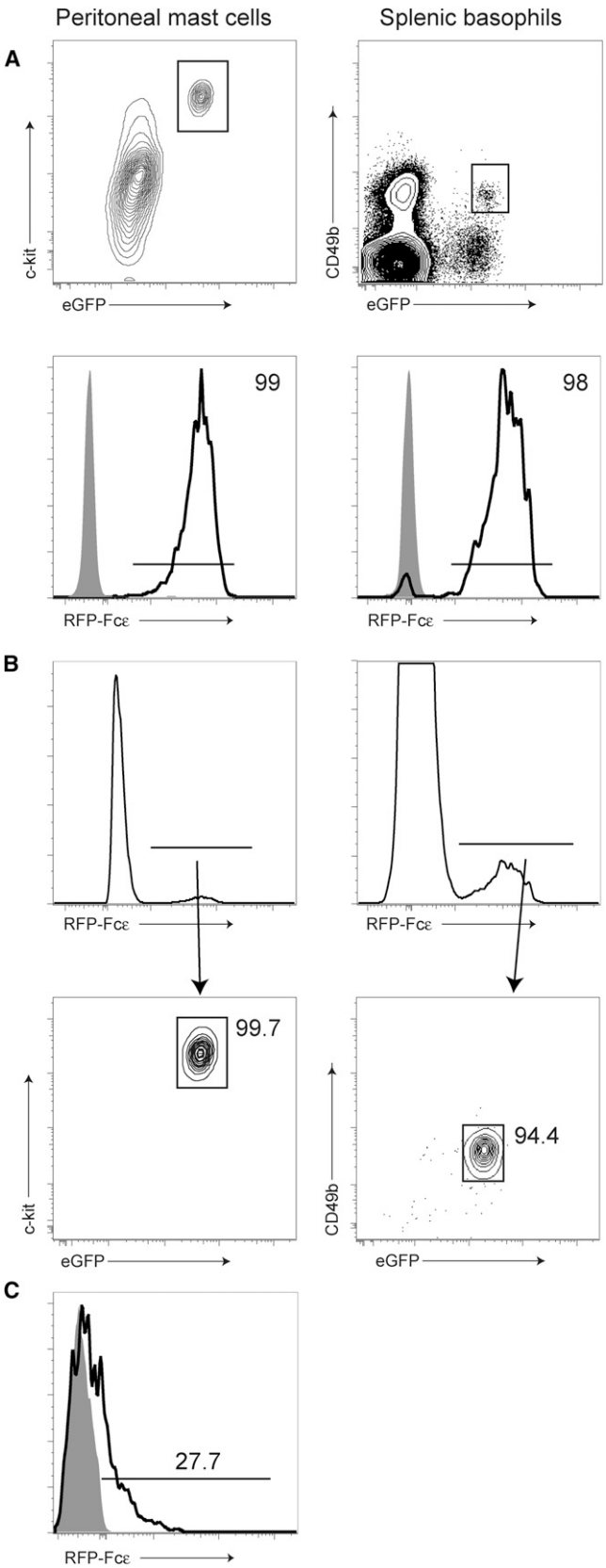

Figure 2. Characterization of RFP-Fcε

(A and B) We isolated peritoneal mast cells (left column) and splenic basophils (right column) from 4get BALB/c mice infused with 1 μg of RFP-Fcε i.v. one day prior. In (A), we gated for c-kit$^+$GFP$^+$ mast cells and CD49b$^+$GFP$^+$ basophils and examined RFP-Fcε capture (bottom row, black histograms). Gray histograms represent similarly gated cells from noninfused mice. In (B), we took total live cells from the peritoneum (left column) or spleen (right column) and analyzed all RFP$^+$ cells. RFP$^+$ cells were then gated on c-kit$^+$GFP$^+$ mast cells (left contour plot) and CD49b$^+$GFP$^+$ basophils (right contour plot). The percent of cells lying in the respective gate is noted.

(C) We isolated ckit$^+$GFP$^+$ ear skin mast cells from 4get BALB/c mice one day following an i.v. 10 μg RFP-Fcε infusion. The black histogram represents the percent RFP$^+$ cells within the indicated gate. The gray histogram represents RFP fluorescence from a noninfused animal.

after a 10 μg i.v. infusion (Figure 2C). Together, these data indicated that RFP-Fcε displays similar binding and distribution characteristics to native IgE.

To visualize the distribution of mast cell IgE uptake, we infused 10 μg RFP-Fcε i.v. into WT or mast cell-deficient *Kit*$^{W\text{-}sh/W\text{-}sh}$ (Sash) mice (Wolters et al., 2005). After 24 hr, we counterstained blood vessels in vivo with i.v. tomato lectin FITC and examined whole mounts of ear tissue by using confocal microscopy (Figure 3A). WT mice showed an abundance of RFP$^+$ cells with most cells lying in a perivascular location. In contrast to WT mice, mast cell-deficient mice demonstrated no RFP$^+$ cells in the ear skin, though RFP$^+$ basophils could be demonstrated within the vasculature (Figure 3A). We next sought to obtain quantitative data to examine whether RFP$^+$ mast cells tended to be closer to blood vessels than the total mast cell pool. When bred to a *cre*-dependent lineage reporter mouse, such as Rosa-YFP (Srinivas et al., 2001), MCPT5cre reporter mice (M5Rosa-YFP) allow specific visualization of >90% of mast cells within the ear skin (Dudeck et al., 2011; Scholten et al., 2008). After infusion with RFP-Fcε, RFP-Fcε was found on ~50% of mast cells (Figure 3B), and some RFP-Fcε$^+$ mast cells appeared to direct cellular projections toward the blood vessel though these initial studies lacked the resolution to define these projections (Figure 3C).

Whereas RFP-Fcε$^+$ and RFP-Fcε$^-$ mast cells were both found to associate with the vasculature, RFP$^+$ mast cells were on average 35% closer to the nearest blood vessel compared to the total mast cell population (Figure 3D). In addition, nearly half of the RFP$^+$ cells were within 2 μm of the nearest blood vessel, whereas only one quarter of the total mast cell population was similarly positioned (Figure 3D). Together, these data indicated that perivascular mast cells preferentially acquire IgE from the blood, and we hypothesized that mast cells might directly sample blood to acquire IgE.

Perivascular Mast Cells Have Access to Blood Contents

We first took a flow cytometric approach to demonstrate that mast cells have direct access to blood contents. Similar to established approaches (Pereira et al., 2009; Zachariah and Cyster, 2010), we infused 4get mice with a c-kit monoclonal antibody (2B8) conjugated to a high molecular weight fluorophore, phycoerythrin (PE). If allowed to circulate for a short period of time, PE-antibody conjugates remain intravascular and binding to target cells requires either direct blood exposure or sampling of intravascular contents. After a 5 min infusion, we observed that

Please cite this article in press as: Cheng et al., Perivascular Mast Cells Dynamically Probe Cutaneous Blood Vessels to Capture Immunoglobulin E, Immunity (2013), http://dx.doi.org/10.1016/j.immuni.2012.09.022

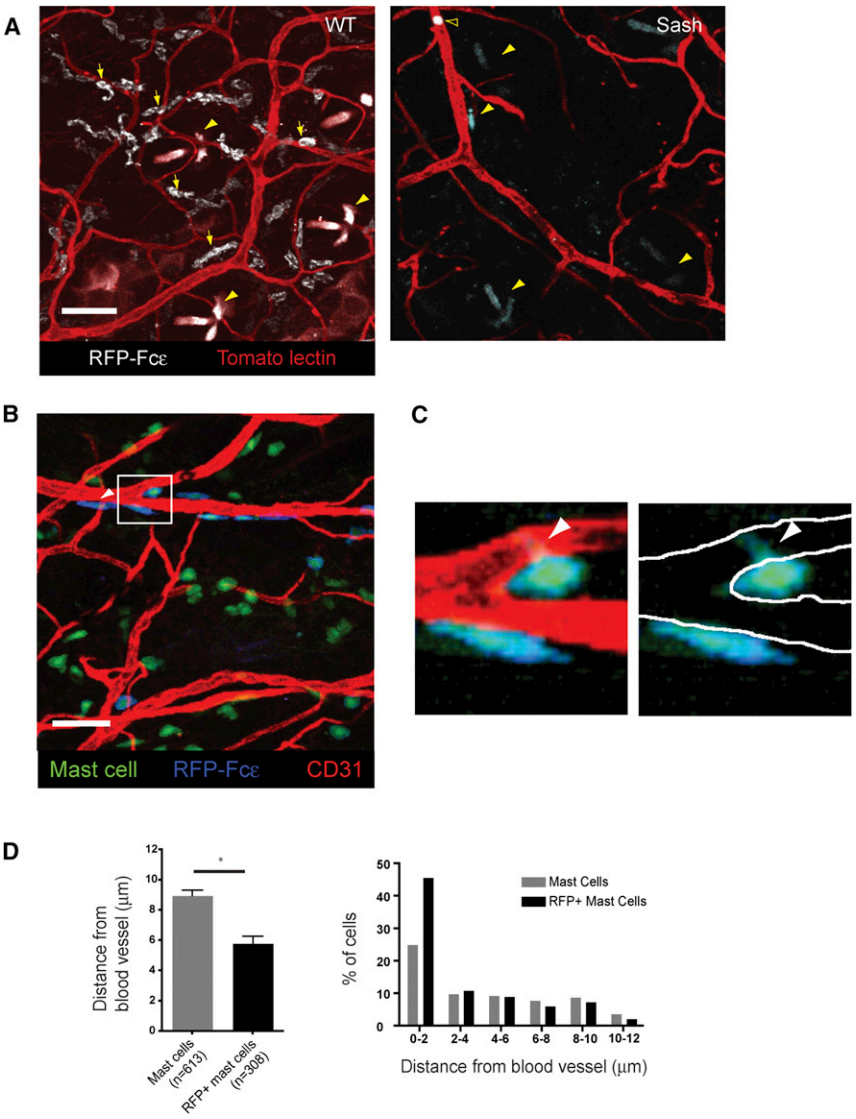

Figure 3. Perivascular Mast Cells Preferentially Capture RFP-Fcε from Blood In Situ

(A) WT or mast cell-deficient (Sash) mice received 10 μg of RFP-Fcε i.v. and were analyzed for RFP-Fcε uptake by confocal microscopy 24 hr later. Images represent 12 and 15 μm z projections from whole mounts of ear tissue. Yellow arrows highlight representative RFP$^+$ mast cells, yellow arrowheads indicate hair follicles, and the open arrowhead in the right panel indicates a basophil. Tomato lectin was used to counterstain blood vessels. Images are representative of results from eight separate mice. Scale bars represent 50 μm.

(B) A maximum intensity projection derived from a 24 μm z stack of ear skin from a M5cre x Rosa-YFP mouse with a z step size of 0.5 μm. The mouse received 10 μg of RFP-Fcε i.v. 1 day prior and anti-CD31 to label blood vessels 10 min prior to analysis. Scale bars represent 50 μm. The white arrowhead highlights a YFP$^+$ mast cell with peripheral RFP-Fcε in blue. Images are representative of ten individual z stacks.

(C) The left panel represents a zoomed in view of the box in 3B. In the right panel, the borders of the blood vessel wall are denoted by white lines with the green projection of the mast cell body within the boundaries of the vessel wall.

(D) Total YFP$^+$ mast cells or RFP$^+$ mast cells from M5cre x Rosa-YFP mice that had received 10 μg of RFP-Fcε i.v. 1 day prior were examined for mean distance from the nearest blood vessel. The left panel depicts the average distance of the indicated mast cell population from the nearest blood vessel, and the right panel represents the percent of mast cells within the indicated distance range from the nearest blood vessel. Four z stacks were analyzed with a total of 613 YFP$^+$ mast cells and 308 RFP$^+$ mast cells. Graph in left panel depicts mean ± SEM. *$p < 0.0001$

approximately 15%–20% of mast cells captured 2B8-PE (Figure 4A). Capture of 2B8-PE was not IgE-dependent because *Fcer1a*$^{-/-}$ mice showed similar 2B8-PE uptake when compared to WT animals.

As noted in our prior experiments, peritoneal mast cells display rapid and uniform acquisition of IgE (Figure 1). To examine whether peritoneal mast cells similarly display direct access to the blood, we assessed 2B8-PE binding in these cells. Consistent with a lack of direct access to the blood and in contrast to ear skin mast cells, peritoneal mast cells showed no binding of 2B8-PE after i.v. exposure (Figure 4B). This was not due to an inherent inability to bind this antibody because intraperitoneal (i.p.) injection of 2B8-PE led to rapid binding to peritoneal mast cells but essentially no binding to skin mast cells (Figure 4B).

We next sought to characterize the positioning and dynamics of mast cell projections and blood vessels (Figure 3B). To investigate this, we employed intravital, high-resolution confocal microscopy in MCPT5-cre x Ai6 mice (M5Ai6), which allowed for greater detail in visualization of mast cells and cellular projections in vivo (Madisen et al., 2010). Similar to our static imaging, we found mast cells closely approximated to blood vessels marked with labeled anti-CD31 antibody (Figure 5A). We observed two distinct probing phenomena. First, some mast cells demonstrated relatively stable projections in the interior of blood vessels (Figure 5A; Movie S1). As we followed such cells in time, serial images demonstrated the retraction of projections (Figure 5B; Movie S2). In Figure 5B, the projection retracted approximately 5 μm over 30 min. We also noted a second behavior in which mast cells serially interacted with the vessel wall and/or the interior of the lumen with portions of the cell body or a cellular projection (Figure 5C; Movie S3).

Because mast cells would not be expected to penetrate blood vessels ensheathed in smooth muscle, including arterioles, we also examined the distribution of mast cells in relation to smooth muscle actin (SMA)-positive vessels. Ear skin whole-mount tissue demonstrated a relative paucity of SMA$^+$ blood vessels at the periphery of the ear where we performed dynamic imaging (Figure S2A). These data indicate that distal ear skin primarily contains capillary beds and smaller venules. Consistent with the representation of SMA$^+$ vessels in the ear skin, mast cells

Please cite this article in press as: Cheng et al., Perivascular Mast Cells Dynamically Probe Cutaneous Blood Vessels to Capture Immunoglobulin E, Immunity (2013), http://dx.doi.org/10.1016/j.immuni.2012.09.022

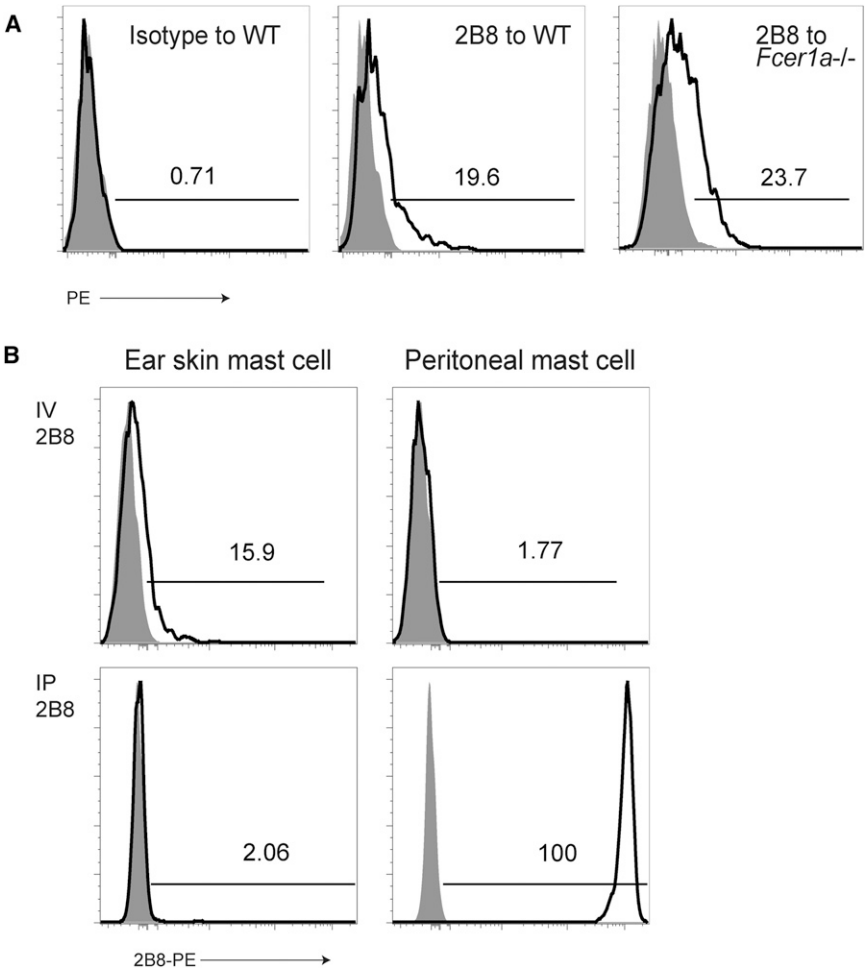

Figure 4. Mast Cells Probe Blood to Access Vascular Contents

(A) Within 5 min after i.v. injection of isotype control (left) or 2B8 (middle and right) antibodies conjugated to PE, we examined c-kit$^+$GFP$^+$ ear skin mast cells for antibody uptake in WT (left and middle) or *Fcer1a*$^{-/-}$ animals (right) from 4get BALB/c mice. Data are representative of three experiments with two to six samples per group. Numbers represent the percent of PE-positive cells in each sample. Shaded histograms represent mice that did not receive labeled antibody.

(B) 4get BALB/c mice received 2B8-PE either i.v. (top row) or i.p. (bottom row), and 5 min later, we examined ear skin (left column) or peritoneal (right column) mast cells for 2B8-PE uptake (black histograms). Gray histograms depict noninfused animals. The percent of cells within the indicated gates are depicted within each plot.

showed a relative absence of disposition toward these vessels as ~3% of mast cells were positioned within 2 μm of SMA$^+$ vessels compared to ~25% found disposed near CD31$^+$ blood vessels in general (Figure S2B). We next examined whether mast cells with recent IgE uptake showed a similar pattern of IgE uptake. After infusion with RFP-Fcε, we stained fixed ear tissue for SMA. Though our analysis was limited by a drop in RFP signal following fixation, we observed that RFP$^+$ cells tended to be in locations remote from SMA$^+$ vessels (Figure S2C).

We next examined fixed ear tissue to further define the entry point of the cellular extensions at the blood vessels. After a brief period of labeling blood vessels in vivo with anti-CD31 monoclonal antibody, we harvested ear tissue and analyzed fixed tissue by using confocal microscopy on ear skin whole mounts. Optical sectioning of the tissue indicated that extensions from the mast cell entered the blood vessel at areas with diminished CD31 staining, suggesting penetration of the vessel lumen (Figures 5D and 5E). In Figure 5E, the extension makes an abrupt turn as it traverses the vessel wall and then associates with the lumen of the vessel wall.

Although our data indicated that mast cell sampling of blood contents is an efficient means for perivascular mast cells to capture free IgE, other mechanisms could also contribute. Loading of monomeric IgE onto mast cells is thought to modulate mast cell function, including the possibility of piecemeal degranulation (Kawakami and Galli, 2002), which could lead to local changes in vasopermeability and increased IgE diffusion. By using cell surface CD107a and diminished side-scatter profile as markers of mast cell activation and degranulation, we examined whether IgE loading on mast cells resulted in changes in either of these parameters (Gekara and Weiss, 2008). To ensure uniform loading of mast cells during the assay, we used peritoneal mast cells as our source of mast cells. Following an i.v. infusion of IgE, peritoneal mast cells demonstrated baseline expression of CD107a and native SSC profiles, which contrasted with control antigen-IgE-activated mast cells (Figure 6A). To directly address the importance of secreted mast cell products, such as histamine, on IgE uptake in skin, we used a pharmacologic approach to block H1 and H2 histamine receptors and mast cell degranulation. IgE loading in ear skin mast cells was not affected by these inhibitors (Figure 6B).

We next wanted to determine whether mast cell projections directly interact with intravascular IgE. Because fluorescence of RFP-Fcε was too insensitive for this application, we developed a technique by using streptavidin-coated beads coupled to biotinylated IgE and a fluorescent dye. After an infusion of 10^9 beads, beads were found in systemic circulation but were cleared within 15 min (data not shown). As a control, we used dye-coated beads. After infusion of control beads into mast cell reporter mice, we found a few beads near perivascular mast cells but no interaction with the bead (Figure 7A; Movie S4). In contrast, mast cells showed interactions with IgE-coated beads in the form of projections extending toward an intravascular bead and engulfing it (Figure 7B; Movies S5 and S6).

To further establish the capacity of mast cells to capture intravascular IgE, we determined the number of IgE-coated beads in

Please cite this article in press as: Cheng et al., Perivascular Mast Cells Dynamically Probe Cutaneous Blood Vessels to Capture Immunoglobulin E, Immunity (2013), http://dx.doi.org/10.1016/j.immuni.2012.09.022

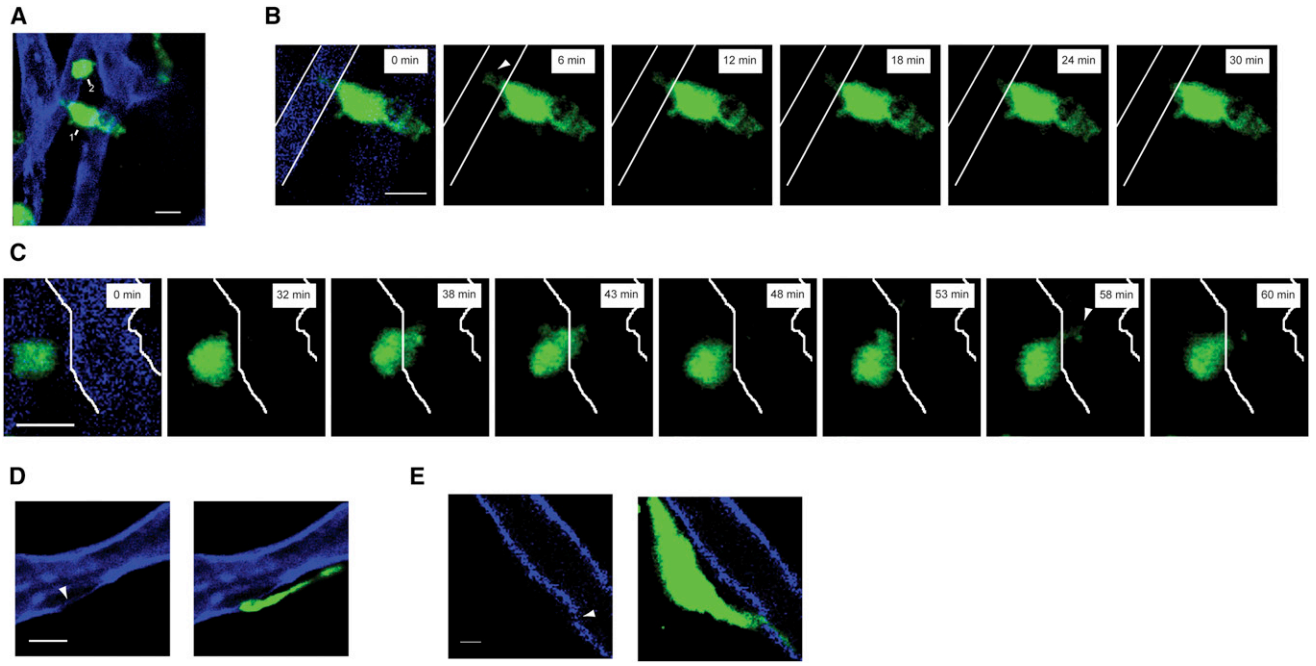

Figure 5. Mast Cells Are Tightly Associated with Blood Vessels and Can Dynamically Sample the Intravascular Lumen

(A) A 25 μm maximum intensity projection of two mast cells (green and labeled 1 or 2). Both mast cells are adjacent to blood vessels (blue). The scale bar is 10 μm. z stack is representative of imaging performed on three individual mice.

(B) Single z slices of Cell 1 in (A) starting at time 0 on the left. The boundaries of the blood vessel are then depicted only as white solid lines for the remainder of the z slices. Each frame is separated by ~6 min and shows the withdrawal of the projection observed at time 0 and highlighted by the white arrowhead in the first panel.

(C) Single z slices of Cell 2 in (A) starting at time 0 on the left. The boundaries of the blood vessel are then depicted only as white solid lines for the remainder of the z slices. Each frame is separated by ~5 min and shows serial interactions between the mast cell and blood vessel with portions of the mast cell body in the vessel lumen at (t = 38 and 43) or a projection directed into the vessel at t = 58). A white arrowhead at t = 58 denotes the mast cell projection.

(D and E) Single optical sections from M5creAi6 mice with CD31-labeled blood vessel in blue and mast cells in green. The left panel depicts the vessel alone, whereas the right panel is merged with the mast cells. The areas of decreased CD31 signal are depicted by the white arrowheads. Scale bar represents 10 μm in (D) and 3 μm in (E).

See also Figure S2 and Movies S1, S2, and S3.

mouse ear skin 20 min after infusion. In mast cell replete mice, we recovered an average of 1,337 beads per mg of ear tissue (Figure 7C). In contrast, mast cell deficient (MCPT5cre x Rosa-DTA) mice exhibited a nearly 70% drop in bead recovery. Together, these data indicate that mast cells interact directly with intravascular contents in a dynamic fashion and selectively remove IgE from blood.

DISCUSSION

The acquisition of IgE by mast cells is central to mast cell function, and the importance of this interaction has been underscored by two recent studies (Dudeck et al., 2011; Feyerabend et al., 2011). Given the critical role of IgE in mast cell biology, our study sought to examine how tissue mast cells acquire IgE. The studies presented here indicate that IgE acquisition by mast cells is regulated at the level of the vasculature with perivascular mast cells demonstrating selective uptake of IgE from the blood. Further understanding into the regulation of mast cell IgE uptake may also provide new therapeutic approaches, as well.

Immune surveillance of intravascular components has been previously described in professional antigen presenting cells (APC), including intra-aortic dendritic cells and Kupffer cells, which also reside within the vasculature (Choi et al., 2009; Lee et al., 2010). Our data illustrate that extravascular cells are also capable of probing blood, akin to sampling of intraluminal contents in the gastrointestinal and respiratory tracts by $CD103^+$ dendritic cells (Chieppa et al., 2006; Lambrecht and Hammad, 2009; Rescigno et al., 2001). Mast cells are not generally considered to be antigen-presenting cells, though mast cells may express MHC class II under specific conditions (Kambayashi et al., 2009). Instead, intravascular sampling appears to be a means for mast cells to capture unbound IgE, which in turn could promote mast cell function and survival (Kawakami and Galli, 2002; Kraft and Kinet, 2007).

Tissue mast cells have long been known to project dendrites, although the function of these projections has not been clear. Beyond sampling blood, mast cells may also extend projections for intercellular communication through a network of cytonemes. The significance of these projections has not been examined in vivo (Fifadara et al., 2010).

We speculate that in addition to capturing IgE, mast cells employ this sampling mechanism as part of a sentinel function in host defense. Localization to barrier surfaces, the capacity to induce immediate inflammatory responses, and the ability to

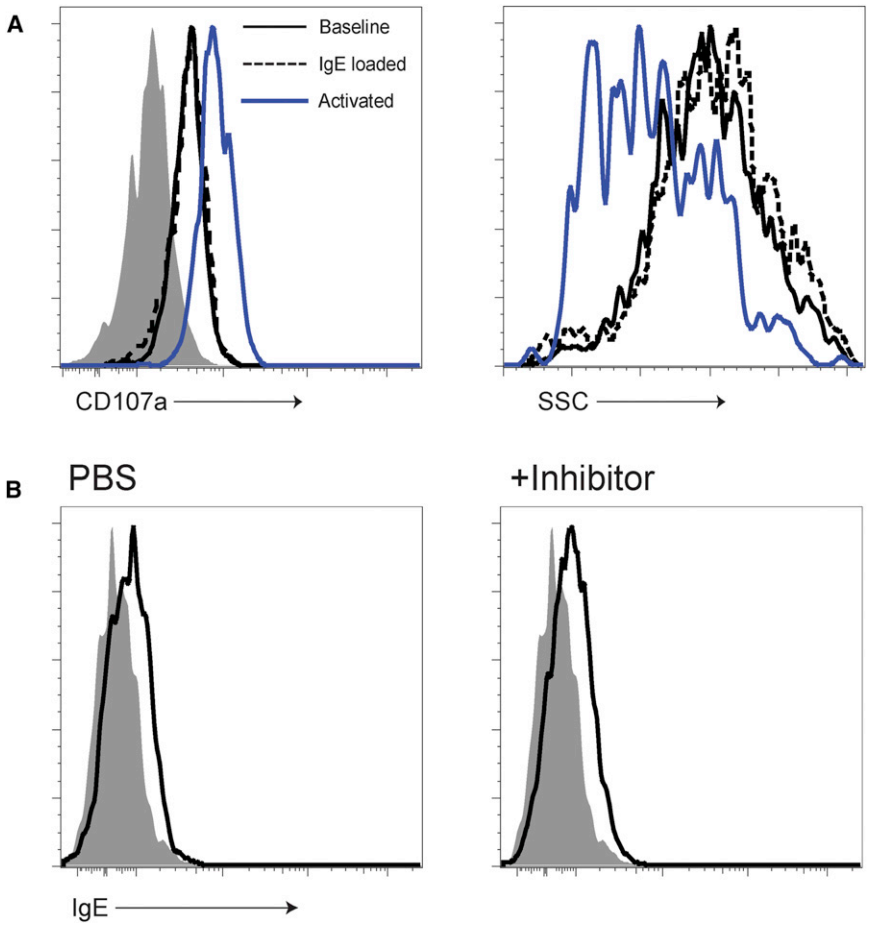

Figure 6. IgE Loading Does Not Cause Degranulation and Is Unaffected by Pharmacologic Inhibition of Mast Cell Function

(A) 4get BALB/c mice received either PBS (solid black line) or monoclonal anti-TNP IgE antibody (dashed line) i.v. Four hours later, surface LAMP-1 (CD107a) and granularity (side scatter) were examined on peritoneal mast cells. An additional control group for mast cell activation is represented by the blue line. This group of mice had been loaded with anti-TNP IgE 1 day prior and challenged with 1 mg of TNP-ovalbumin at the start of the experiment. These activated mast cells demonstrate increased LAMP-1 staining after activation as well as a drop in side-scatter (SSC). By contrast, IgE-loaded mast cells show equivalent LAMP-1 and SSC profiles compared to controls. The gray histogram in the left panel represents isotype control staining.

(B) 4getx*Rag2*$^{-/-}$ mice were pretreated with PBS (left panel) or a combination of pyrilamine, ranitidine, and cromolyn sodium (right panel). Mice were then loaded with 10 μg of monoclonal IgE antibody and ear mast cells assessed for IgE uptake 24 hr later.

recruit additional immune cells, positions mast cells as initial responders to pathogen invasion. Specific IgE further enhances these functions when antigen is present. Although local production of IgE has been described in the airway mucosa (Gould and Sutton, 2008), delivery to the skin and mucosal sites remote from IgE production requires systemic distribution. The surveillance mechanism we describe limits distribution of IgE to subsets of mast cells in close approximation to the vasculature. Thus, the cells most likely to influence vascular permeability after activation also have the greatest access to free IgE. It remains unclear whether this anatomic positioning also defines subsets of mast cells that have functional differences beyond the effects of IgE.

Our studies focus on the steady-state means by which mast cells acquire IgE. Local changes in vascular permeability, which could be seen with immediate hypersensitivity reactions, infection, or dermatitis, may further modulate IgE loading. In addition, the disparate mechanisms by which skin and peritoneal mast cells acquire IgE suggest that IgE uptake may be organ-specific. Several factors, including mast cell positioning, local vascular permeability, and the predominant mast cell populations (connective tissue versus mucosal) contained within each organ may all play a role in IgE acquisition.

Our data uncover a regulated means by which mast cells acquire IgE and fill an important gap in our understanding of the steps required in the elicitation of hypersensitivity by mast cells. The molecular mechanism by which mast cells survey blood remains undefined. We hypothesize that a gradient between blood and tissue of a particular factor or family of molecules may drive mast cell sampling behavior. Further understanding of the mechanism by which mast cells survey the blood compartment may provide a means to modulate human allergic disease in the future.

EXPERIMENTAL PROCEDURES

Mice

4get BALB/c and IgE-deficient 4getx*Rag2*$^{-/-}$ mice have been described (Cheng et al., 2010; Mohrs et al., 2001). Mast cell-deficient *Kit*$^{W\text{-}sh/W\text{-}sh}$ (Sash) mice on a C57BL/6 background were provided by G. Caughey (UCSF). MCPT5 Cre mice were bred to either of the following reporter mice: Rosa-YFP, Ai6, or Rosa-DTA (Madisen et al., 2010; Srinivas et al., 2001; Voehringer et al., 2008). Rosa-YFP and Ai6 mice were obtained from Jackson Laboratories (Bar Harbor, ME). Mice were housed in Specific Pathogen Free facilities. Experimental mice were 8–10 weeks old. Animal use was governed by and in accordance with approved protocols overseen by the Laboratory Animal Resource Center (LARC) and Institutional Animal Care and Use Committee (IACUC) at UCSF.

Skin Tissue and Peritoneal Mast Cell Isolation

Ear tissue from euthanized mice was split into dorsal and ventral halves and then minced. Tissue was resuspended in PBS plus 2 U/ml of Liberase CI (Roche) and incubated at 37°C for 45 min in an orbital shaker similar to published protocols (Grimbaldeston et al., 2007). Collagenase activity was quenched with PBS supplemented with 2% fetal calf serum (FCS), and the cells were analyzed by flow cytometry. Peritoneal mast cells were analyzed from lavage fluid collected after euthanasia. The gating scheme was similar to a previously published study (Gessner et al., 2005).

Please cite this article in press as: Cheng et al., Perivascular Mast Cells Dynamically Probe Cutaneous Blood Vessels to Capture Immunoglobulin E, Immunity (2013), http://dx.doi.org/10.1016/j.immuni.2012.09.022

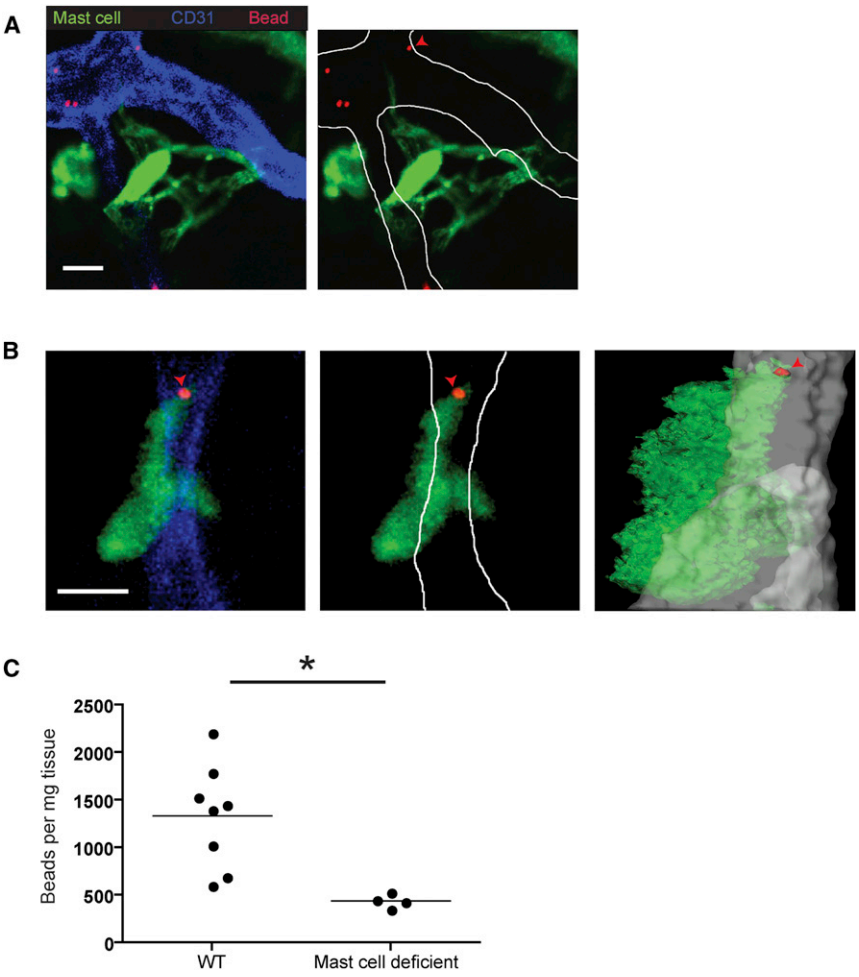

Figure 7. Mast Cells Capture Intravascular IgE-Coated Beads

(A) A single z slice depicting a mast cell (green) directing projections into a blood vessel (blue) but not interacting with fluorescent beads (red). Ten minutes prior to imaging, the M5cre x Ai6 mast cell reporter mouse received $\sim 10^9$ rhodamine-coated beads i.v. Scale bar represents 10 μm. The left panel shows the native image, whereas the right panel highlights the boundaries of the vessel with improved visualization of the projections. Images are representative of five individual imaging volumes. One of the IgE beads is also denoted by a red arrowhead in the right panel.

(B) A single z slice illustrating a mast cell (green) directing a projection into a blood vessel (blue) and interacting with an IgE bead (red) distally. The IgE bead is also denoted by the red arrowhead. Ten minutes prior to imaging, the M5cre x Ai6 mast cell reporter mouse received $\sim 10^9$ IgE and rhodamine-coated beads i.v. The left panel shows the native image, whereas the middle panel highlights the boundaries of the blood vessel. The right panel is an orthogonal view of the z stack. The mast cell (green), bead (red), and blood vessel (gray) have been rendered into surfaces. Scale bar represents 10 μm. Images are representative of five individual imaging volumes.

(C) Approximately 10^9 IgE coated beads were infused i.v. into WT or mast cell-deficient (M5creDTA) mice and subsequently isolated from ear tissue after weighing. The number of beads is represented as the number of beads per mg of ear tissue. *$p < 0.01$.

See also Movies S4, S5, and S6.

Construction of RFP-Fcε

RFP-Fcε was constructed and produced in the same manner as previous molecules (Cheng et al., 2010). A primer pair (5′- TTTAGATCTGTGAGC AAGGGCGAGG-3′ and 5′-TGGATCCCTTGTACAGCTCGTCCATGC-3′) that spanned amino acids 2–476 was used to amplify the tdRFP cDNA (Shaner et al., 2004).

Antibodies and Flow Cytometry

For mast cell staining, we used the following antibody clones: c-kit (ACK2, eBioscience, San Diego, CA), FcεRI (Mar-1, eBioscience). For basophil staining, we used CD49b (DX5, eBioscience). For in vivo infusion, the following antibodies and clones were used: mouse IgE C38-2 (BD PharMingen, San Diego, CA) anti-CD31 APC (390, eBioscience), tomato lectin FITC (Vector Labs, Burlingame, CA), anti-c-kit PE (2B8, eBioscience). For flow cytometry, we used an LSRII (Becton Dickinson, San Jose, CA) for data acquisition and analysis. We performed postacquisition analysis by using FlowJo software (Treestar, Ashland, OR).

Mast Cell Blood Sampling

One microgram of PE-conjugated 2B8 or isotype control rat IgG2b antibody was infused i.v. into the tail veins of mice. Within 5 min, mice were euthanized with immediate processing of tissue for flow cytometry. Statistical analysis was performed by using an unpaired t test.

Confocal Microscopy

For confocal microscopy, ear tissue from euthanized mice was split into dorsal and ventral halves (except for experiments involving bead infusions for which the ears remained intact). The tissue was then bathed in Vectashield (Vector Labs) and analyzed with a Nikon C1si laser scanning confocal microscope. Images were analyzed and rendered by using Imaris software (Bitplane, Zurich, Switzerland). To analyze the distance from mast cells to blood vessels, we used Imaris software to mark the boundaries of the blood vessels and to generate "spots" to represent index populations. The software then calculated the distance from the center of each of these spots to the edge of the nearest blood vessel. A Student's t test was performed for significance on the resulting data sets. For fixed tissues, mice were fixed with 4% paraformaldehyde in PBS for 2 hr on ice. Samples were then washed and analyzed as above.

Intravital Microscopy

Mice received intraperitoneal injections of ketamine and xylazine for anesthesia. Mice were then placed in a lateral decubitus position on the imaging stage of a Nikon C1si microscope. The ventral half of the ear was then dissected away with preservation of blood flow to the dorsal half verified under light microscopy. The mouse was then secured on the stage with the microscope objective directed toward the dermal surface. Images were compiled, analyzed, and rendered by using Imaris software (Bitplane, Zurich, Switzerland).

IgE Beads

Monoclonal, anti-trinitrophenol IgE (C38-2) was biotinylated with EZ-Link Sulfo NHS (Thermo Scientific, Rockford, IL). After purification (Zeba Spin Desalting columns, Thermo Scientific), 40 μg of IgE (4B12, Vector Labs) was then combined with $\sim 10^9$ Dynal MyOne T1 streptavidin beads for 15 min (Invitrogen, Carlsbad, CA). To quench unoccupied streptavidin moieties and label the

bead, 40 μg of dextran (3 kDa) coupled to biotin and tetramethylrhodamine was added to the mixture for 15 min (Invitrogen). The beads were then washed and resuspended in PBS prior to i.v. infusion. Ten minutes after infusion, ears were dissected from euthanized mice and analyzed intact by using confocal microscopy. For the bead recovery assay, ears were harvested 20 min after infusion, weighed, and placed directly into digest buffer (0.25% SDS, 0.1 M NaCl, 50 mM Tris pH 8, 7.5 mM EDTA) with an additional 0.5 mg/ml Proteinase K for 3 hr at 56 degrees and constant agitation. Magnetic beads were then isolated by using a Dynal magnet (Invitrogen, Carlsbad, CA) after multiple washes with PBS and resuspended in 100 μl of water. The beads were then counted manually with a hemacytometer.

LAMP-1 Staining

Four hours after i.v. IgE infusion or i.p. challenge with 1 mg of TNP-ovalbumin in sensitized animals, peritoneal lavage fluid was isolated and ckit^{+}GFP^{+} mast cells were stained with anti-CD107a (1D4B, eBioscience).

Histamine Blockade and Cromolyn Sodium Administration

Mice received inhibitors of mast cell degranulation (cromolyn) and histamine blockade per published protocols (Dawicki et al., 2010).

SUPPLEMENTAL INFORMATION

Supplemental Information includes two figures, Supplemental Experimental Procedures, and six movies and can be found with this article online at http://dx.doi.org/10.1016/j.immuni.2012.09.022.

ACKNOWLEDGMENTS

This work was supported by the following grants to R.M.L.: the Howard Hughes Medical Institute, NIH AI026918, AI30663, AI078869, and SABRE Center at UCSF; the following grants to L.E.C.: NIH T32 (HD044331), AAAAI-GSK Career Development Award, the A.P. Giannini Medical Research Foundation, and NIH AI095319; and the following grants to K.H.: the German Research Council (DFG; CRC/SFB832, project A14) and the German-Israeli Foundation for Scientific Research and Development (993/2008). We thank C. Allen and G. Caughey for providing mice and the Biological Imaging Development Center for assistance with microscopy. We thank members of the Locksley laboratory, C. Allen, J. Cyster, and S. Coughlin for thoughtful discussions and/or review of the manuscript. We also thank P. Kubes for sharing experimental protocols.

Received: January 31, 2012
Accepted: September 26, 2012
Published: January 3, 2013

REFERENCES

Cheng, L.E., Wang, Z.E., and Locksley, R.M. (2010). Murine B cells regulate serum IgE levels in a CD23-dependent manner. J. Immunol. *185*, 5040–5047.

Chieppa, M., Rescigno, M., Huang, A.Y., and Germain, R.N. (2006). Dynamic imaging of dendritic cell extension into the small bowel lumen in response to epithelial cell TLR engagement. J. Exp. Med. *203*, 2841–2852.

Choi, J.H., Do, Y., Cheong, C., Koh, H., Boscardin, S.B., Oh, Y.S., Bozzacco, L., Trumpfheller, C., Park, C.G., and Steinman, R.M. (2009). Identification of antigen-presenting dendritic cells in mouse aorta and cardiac valves. J. Exp. Med. *206*, 497–505.

Dawicki, W., Jawdat, D.W., Xu, N., and Marshall, J.S. (2010). Mast cells, histamine, and IL-6 regulate the selective influx of dendritic cell subsets into an inflamed lymph node. J. Immunol. *184*, 2116–2123.

Dudeck, A., Dudeck, J., Scholten, J., Petzold, A., Surianarayanan, S., Köhler, A., Peschke, K., Vöhringer, D., Waskow, C., Krieg, T., et al. (2011). Mast cells are key promoters of contact allergy that mediate the adjuvant effects of haptens. Immunity *34*, 973–984.

Feyerabend, T.B., Weiser, A., Tietz, A., Stassen, M., Harris, N., Kopf, M., Radermacher, P., Möller, P., Benoist, C., Mathis, D., et al. (2011). Cre-mediated cell ablation contests mast cell contribution in models of antibody- and T cell-mediated autoimmunity. Immunity *35*, 832–844.

Fifadara, N.H., Beer, F., Ono, S., and Ono, S.J. (2010). Interaction between activated chemokine receptor 1 and FcepsilonRI at membrane rafts promotes communication and F-actin-rich cytoneme extensions between mast cells. Int. Immunol. *22*, 113–128.

Galli, S.J., and Tsai, M. (2010). Mast cells in allergy and infection: versatile effector and regulatory cells in innate and adaptive immunity. Eur. J. Immunol. *40*, 1843–1851.

Gekara, N.O., and Weiss, S. (2008). Mast cells initiate early anti-Listeria host defences. Cell. Microbiol. *10*, 225–236.

Gessner, A., Mohrs, K., and Mohrs, M. (2005). Mast cells, basophils, and eosinophils acquire constitutive IL-4 and IL-13 transcripts during lineage differentiation that are sufficient for rapid cytokine production. J. Immunol. *174*, 1063–1072.

Gould, H.J., and Sutton, B.J. (2008). IgE in allergy and asthma today. Nat. Rev. Immunol. *8*, 205–217.

Grimbaldeston, M.A., Nakae, S., Kalesnikoff, J., Tsai, M., and Galli, S.J. (2007). Mast cell-derived interleukin 10 limits skin pathology in contact dermatitis and chronic irradiation with ultraviolet B. Nat. Immunol. *8*, 1095–1104.

Hallgren, J., and Gurish, M.F. (2007). Pathways of murine mast cell development and trafficking: tracking the roots and routes of the mast cell. Immunol. Rev. *217*, 8–18.

Kambayashi, T., Allenspach, E.J., Chang, J.T., Zou, T., Shoag, J.E., Reiner, S.L., Caton, A.J., and Koretzky, G.A. (2009). Inducible MHC class II expression by mast cells supports effector and regulatory T cell activation. J. Immunol. *182*, 4686–4695.

Kawakami, T., and Galli, S.J. (2002). Regulation of mast-cell and basophil function and survival by IgE. Nat. Rev. Immunol. *2*, 773–786.

Kraft, S., and Kinet, J.P. (2007). New developments in FcepsilonRI regulation, function and inhibition. Nat. Rev. Immunol. *7*, 365–378.

Lambrecht, B.N., and Hammad, H. (2009). Biology of lung dendritic cells at the origin of asthma. Immunity *31*, 412–424.

Lee, W.Y., Moriarty, T.J., Wong, C.H., Zhou, H., Strieter, R.M., van Rooijen, N., Chaconas, G., and Kubes, P. (2010). An intravascular immune response to Borrelia burgdorferi involves Kupffer cells and iNKT cells. Nat. Immunol. *11*, 295–302.

Locksley, R.M. (2010). Asthma and allergic inflammation. Cell *140*, 777–783.

Luger, E.O., Fokuhl, V., Wegmann, M., Abram, M., Tillack, K., Achatz, G., Manz, R.A., Worm, M., Radbruch, A., and Renz, H. (2009). Induction of long-lived allergen-specific plasma cells by mucosal allergen challenge. J. Allergy Clin. Immunol. *124*, 819–826.

Madisen, L., Zwingman, T.A., Sunkin, S.M., Oh, S.W., Zariwala, H.A., Gu, H., Ng, L.L., Palmiter, R.D., Hawrylycz, M.J., Jones, A.R., et al. (2010). A robust and high-throughput Cre reporting and characterization system for the whole mouse brain. Nat. Neurosci. *13*, 133–140.

McMenamin, C., Girn, B., and Holt, P.G. (1992). The distribution of IgE plasma cells in lymphoid and non-lymphoid tissues of high-IgE responder rats: differential localization of antigen-specific and 'bystander' components of the IgE response to inhaled antigen. Immunology *77*, 592–596.

Mohrs, M., Shinkai, K., Mohrs, K., and Locksley, R.M. (2001). Analysis of type 2 immunity in vivo with a bicistronic IL-4 reporter. Immunity *15*, 303–311.

Pereira, J.P., An, J., Xu, Y., Huang, Y., and Cyster, J.G. (2009). Cannabinoid receptor 2 mediates the retention of immature B cells in bone marrow sinusoids. Nat. Immunol. *10*, 403–411.

Rescigno, M., Urbano, M., Valzasina, B., Francolini, M., Rotta, G., Bonasio, R., Granucci, F., Kraehenbuhl, J.P., and Ricciardi-Castagnoli, P. (2001). Dendritic cells express tight junction proteins and penetrate gut epithelial monolayers to sample bacteria. Nat. Immunol. *2*, 361–367.

Scholten, J., Hartmann, K., Gerbaulet, A., Krieg, T., Müller, W., Testa, G., and Roers, A. (2008). Mast cell-specific Cre/loxP-mediated recombination in vivo. Transgenic Res. *17*, 307–315.

Shaner, N.C., Campbell, R.E., Steinbach, P.A., Giepmans, B.N., Palmer, A.E., and Tsien, R.Y. (2004). Improved monomeric red, orange and yellow fluorescent proteins derived from Discosoma sp. red fluorescent protein. Nat. Biotechnol. *22*, 1567–1572.

Srinivas, S., Watanabe, T., Lin, C.S., William, C.M., Tanabe, Y., Jessell, T.M., and Costantini, F. (2001). Cre reporter strains produced by targeted insertion of EYFP and ECFP into the ROSA26 locus. BMC Dev. Biol. *1*, 4.

Talay, O., Yan, D., Brightbill, H.D., Straney, E.E., Zhou, M., Ladi, E., Lee, W.P., Egen, J.G., Austin, C.D., Xu, M., and Wu, L.C. (2012). IgE^{+} memory B cells and plasma cells generated through a germinal-center pathway. Nat. Immunol. *13*, 396–404.

Voehringer, D., Liang, H.E., and Locksley, R.M. (2008). Homeostasis and effector function of lymphopenia-induced "memory-like" T cells in constitutively T cell-depleted mice. J. Immunol. *180*, 4742–4753.

Wolters, P.J., Mallen-St Clair, J., Lewis, C.C., Villalta, S.A., Baluk, P., Erle, D.J., and Caughey, G.H. (2005). Tissue-selective mast cell reconstitution and differential lung gene expression in mast cell-deficient Kit(W-sh)/Kit(W-sh) sash mice. Clin. Exp. Allergy *35*, 82–88.

Yamaguchi, M., Lantz, C.S., Oettgen, H.C., Katona, I.M., Fleming, T., Miyajima, I., Kinet, J.P., and Galli, S.J. (1997). IgE enhances mouse mast cell Fc(epsilon)RI expression in vitro and in vivo: evidence for a novel amplification mechanism in IgE-dependent reactions. J. Exp. Med. *185*, 663–672.

Yang, Z., Sullivan, B.M., and Allen, C.D. (2012). Fluorescent in vivo detection reveals that IgE(+) B cells are restrained by an intrinsic cell fate predisposition. Immunity *36*, 857–872.

Zachariah, M.A., and Cyster, J.G. (2010). Neural crest-derived pericytes promote egress of mature thymocytes at the corticomedullary junction. Science *328*, 1129–1135.